

Anharmonic melting of the charge density wave in single-layer TiSe₂

Jianqiang Sky Zhou,^{1,*} Lorenzo Monacelli,² Raffaello Bianco,³
Ion Errea,^{3,4,5} Francesco Mauri,^{2,6} and Matteo Calandra^{1,†}

¹*Sorbonne Université, CNRS, Institut des Nanosciences de Paris, UMR7588, F-75252, Paris, France*

²*Dipartimento di Fisica, Università di Roma Sapienza, Piazzale Aldo Moro 5, I-00185 Roma, Italy*

³*Centro de Física de Materiales (CSIC-UPV/EHU), Manuel de Lardizabal
pasealekua 5, 20018 Donostia-San Sebastián, Basque Country, Spain*

⁴*Fisika Aplikatua 1 Saila, Gipuzkoako Ingeniaritza Eskola, University of the Basque Country
(UPV/EHU), Europa Plaza 1, 20018, Donostia-San Sebastián, Basque Country, Spain*

⁵*Donostia International Physics Center (DIPC), Manuel de Lardizabal
pasealekua 4, 20018 Donostia-San Sebastián, Basque Country, Spain*

⁶*Graphene Labs, Fondazione Istituto Italiano di Tecnologia, Via Morego, I-16163 Genova, Italy*

(Dated: October 29, 2019)

Low dimensional systems with a vanishing band-gap and a large electron-hole interaction have been proposed to be unstable towards exciton formation. As the exciton binding energy increases in low dimension, conventional wisdom suggests that excitonic insulators should be more stable in 2D than in 3D. Here we study the effects of the electron-hole interaction and anharmonicity in single-layer TiSe₂. We find that, contrary to the bulk case and to the generally accepted picture, the electron-hole exchange interaction is much smaller in 2D than in 3D and it has negligible effects on phonon spectra. By calculating anharmonic phonon spectra within the stochastic self-consistent harmonic approximation, we obtain $T_{\text{CDW}} \approx 440\text{K}$ for an isolated and undoped single-layer and $T_{\text{CDW}} \approx 364\text{K}$ for an electron-doping $n = 4.6 \times 10^{13} \text{ cm}^{-2}$, close to the experimental result of 200 – 280K on supported samples. Our work demonstrates that anharmonicity and doping melt the charge density wave in single-layer TiSe₂.

The occurrence of charge ordering in bulk TiSe₂ (see Fig. 1) and its possible interplay with electronic excitations has attracted increasing interest over the last years. Two scenarios for the occurrence of the charge density wave (CDW) have been proposed: the first one is purely electronic and is based on exciton condensation [1–5], while in the second the lattice plays a dominant role via the electron-phonon interaction [6–8]. However, both scenarios are incomplete, as there are currently no explanations of the strong temperature dependence of phonon spectra in the high- T [7] and low- T phases [9, 10] and of the magnitude of T_{CDW} . Surprisingly, little is known about anharmonicity and its effect on the CDW in TiSe₂.

From the theoretical point of view, it has been shown that harmonic calculations in bulk TiSe₂ including the electron-phonon interaction within density-functional perturbation theory (DFPT) [11] correctly reproduce the occurrence of a CDW with a $2 \times 2 \times 2$ periodicity [6, 8, 12]. However, the electronic structures of the high- and low- T phases as well as Raman and infrared spectra of the low- T phase at $T = 0\text{K}$ can only be explained by including the electron-hole exchange interaction within hybrid functionals [8]. Density functional theory (DFT) with semi-local kernels leads to a metallic electronic structure, in disagreement with the angle-resolved photoemission spectroscopy (ARPES) experiments [6, 12, 13] that show a weakly doped semiconductor in both phases. Moreover, they underestimate the square of the electron-phonon deformation potential of a factor of 3 [8].

Recently, single-layer TiSe₂ was synthesized either by exfoliation or molecular beam epitaxy (MBE). It displays a 2×2 CDW with a T_{CDW} that is enhanced with re-

spect to the bulk case ($T_{\text{CDW}}^{\text{bulk}} \approx 200\text{K}$) and is strongly substrate dependent [14–20]: single-layer TiSe₂ on top of insulating MoS₂ has $T_{\text{CDW}} = 280\text{K}$ [14], while on top of n -doped bilayer graphene or highly oriented pyrolytic graphite (HOPG) [14, 18–20] $T_{\text{CDW}} = 200 - 230\text{K}$. This strong variability of T_{CDW} has been tentatively ascribed to the different substrate dielectric constants in possible relation with an excitonic insulator picture [14]. Indeed, as the exciton binding energy increases in low dimension [1–4, 21], conventional wisdom suggests that excitonic insulators should be more stable in 2D than in 3D. However, other effects such as charge transfer from the substrate, the non-stoichiometry due to Se vacancies or doping could be very relevant. From theory, on the one hand the T_{CDW} of TiSe₂ monolayer has up to now only been estimated from a variation of the electronic temperature T_e . At the harmonic level this assumption predicts a $T_{\text{CDW}} \approx 1195\text{K}$ within PBE and $T_{\text{CDW}} \approx 1920\text{K}$ by including the exchange interaction via HSE06 [22], in complete disagreement with the experimental data and leading to an incorrect estimation of T_{CDW} of at least a factor of 5. On the other hand, little is known about the effects of electron-hole exchange interaction on the vibrational properties of single-layer TiSe₂ and its dependence on doping. It has been shown that, neglecting the spin-orbit coupling, semi-local functionals are successful in reproducing the semiconducting state of the low- T phase [23], contrary to what happens in the bulk case.

In this work we study the anharmonic phonon spectra of an isolated single-layer TiSe₂ within the stochastic self-consistent harmonic approximation (SSCHA) [24–27] that has been successfully applied to study the an-

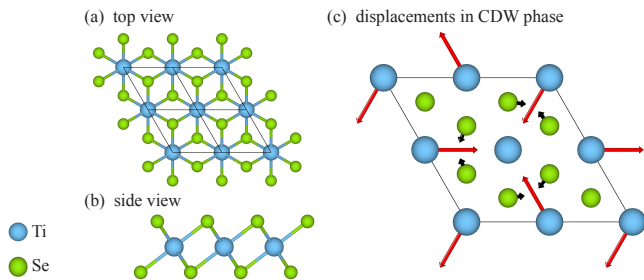


FIG. 1. (a) and (b): top and side schematic views of crystal structure of monolayer TiSe₂ in the high-*T* phase on a 2 × 2 cell. (c): top view of the atomic displacements of the low-*T* phase (i.e., the CDW phase) with respect to the high-*T* phase. Blue and green balls represent Ti and Se atoms, respectively.

harmonicity of other transition metal dichalcogenides [28, 29]. In particular, by including the exchange interaction via semi-local and hybrid functionals [30], we determine the CDW transition and demonstrate that its melting is determined by the combined effect of phonon-phonon scattering and electron doping and not by an excitonic mechanism.

ARPES measurements show that the high-*T* phase of single-layer TiSe₂ is a weakly *n*-doped semiconductor [18, 19, 31] with a 0.098 eV indirect band gap between the Γ (i.e., derived from Se $4p_{xy}$ states) and M (i.e., derived from Ti $3d$ states) points in the Brillouin zone (BZ). In Fig. 2 (a) the calculated electronic band structures in both PBE and HSE06 approximations are presented. PBE predicts a metallic state with a negative band gap of -0.45 eV between the Γ and M points in BZ, in good agreement with previous calculations [23, 32, 33] but in disagreement with ARPES. The HSE06 yields a positive band gap of 0.092 eV, in perfect agreement with ARPES.

The PBE and HSE06 harmonic phonon dispersion are very similar, despite a different electronic structure, as shown in Fig. 2 (b). The A_{1u} mode at the M point is strongly unstable (imaginary phonon frequencies are represented as negative values in all dispersion plots), indicating formation of a 2 × 2 superstructure. The two functionals lead to ≈ 20 cm⁻¹ (i.e., 12%) difference in the A_{1u} imaginary phonon frequency. Other modes at higher energy suffer of a somewhat stronger renormalization. In order to understand if the effect of exchange on the CDW is small, we also calculate the energy gain with respect to the displacement of Ti atoms corresponding to the CDW pattern (see Fig. 1) using the experimental ratio $\delta\text{Ti}/\delta\text{Se} = 3$ [20, 34], as shown in the inset of Fig. 2 (b). Again, the two approximations yield a similar minimum indicating a similar CDW instability, which eventually confirms the negligible effect of electron-hole exchange in the soft-mode harmonic phonon bands. Interestingly, also the position of the energy minimum versus δTi is practically the same, indicative of an akin CDW structure. Note that in bulk TiSe₂, the energy gain for a distortion having modulation $\mathbf{q} = \Gamma\mathbf{L}$ in HSE06 is approximately three

times larger than the PBE one [8] and the minimum occurs at substantially larger δTi in HSE06 than in PBE.

This puzzling difference between bulk and single layer can be understood by noting that in the former the strong electron-hole interaction is between the $4p_{xy}$ occupied states at zone center and some of the empty Ti $3d$ states at the L point. In the bulk, for a distortion having periodicity $\mathbf{q} = \Gamma\mathbf{M}$ (i.e., all the TiSe₂ layers distort in phase), and coupling the Brillouin zone regions around the A point with those around the L point, the energy gain by the distortion is reversed with respect to the case of a distortion having modulation $\mathbf{q} = \Gamma\mathbf{L}$, namely the PBE energy gain is much larger than the HSE06 one [22]. Thus, in the bulk, the exchange interaction effects depend crucially on the modulation of the distortion and on the electronic states involved. In the single layer, the electronic structure of the high-*T* phase along $\Gamma\mathbf{M}$ is very similar to the one of the undistorted bulk along the A-L line, with Γ and M in the single layer corresponding A and L in the bulk. For this reason, the effect of the exchange interaction on the phonon dispersion is much weaker for a $\mathbf{q} = \Gamma\mathbf{M}$ modulation in the single layer than for the case of a $\mathbf{q} = \Gamma\mathbf{L}$ distortion on the bulk. On top of that, other effects contribute to the different energy gain by the $\mathbf{q} = \Gamma\mathbf{M}$ distortion in bulk and single layer, such as the weak but non-negligible band dispersion along k_z close to the A and L high symmetry points in the bulk and the slightly different fillings of the Ti *d*-band at L in the bulk and M in the single layer. This explains why in single layer the effects of exchange on the charge density wave distortion are negligible and demonstrates how simple arguments based on isotropic coulomb interactions [1–4, 21] do not apply easily in layered materials with weak interlayer binding, such as TiSe₂.

Even if the two functionals give practically identical energy versus displacement profiles, this is not enough to conclude that the exchange interaction is irrelevant for the soft mode at the anharmonic level. For this purpose, we calculate the phonon dispersion including non-perturbative anharmonic effects within the SSCHA using both HSE06 and PBE as force engines. Namely, we evaluate the temperature dependent dynamical matrix $\mathbf{D} = \mathbf{M}^{-\frac{1}{2}} \left. \frac{\partial^2 F}{\partial \mathbf{R} \partial \mathbf{R}} \right|_{\mathcal{R}_{eq}} \mathbf{M}^{-\frac{1}{2}}$ where \mathbf{M} is the matrix of the ionic masses M_a with $M_{ab} = \delta_{ab} M_a$ within the SSCHA. The free energy curvature with respect to the vector of the centroid positions \mathcal{R} reads [25]:

$$\frac{\partial^2 F}{\partial \mathbf{R} \partial \mathbf{R}} = \Phi + \overset{(3)}{\Phi} \Lambda(0) \overset{(3)}{\Phi} + \overset{(3)}{\Phi} \Lambda(0) \Theta \Lambda(0) \overset{(3)}{\Phi}, \quad (1)$$

where Φ represents the SSCHA force constant, $\overset{(3)}{\Phi} \Lambda(0) \overset{(3)}{\Phi}$ is the so-called “static bubble term”, and $\overset{(3)}{\Phi} \Lambda(0) \Theta \Lambda(0) \overset{(3)}{\Phi}$ contains the higher order terms. Here $\overset{(n)}{\Phi}$ refers to the *n*-th order anharmonic force constants averaged over the density matrix of the SSCHA hamiltonian (see Ref. [25] for more details on notation). All

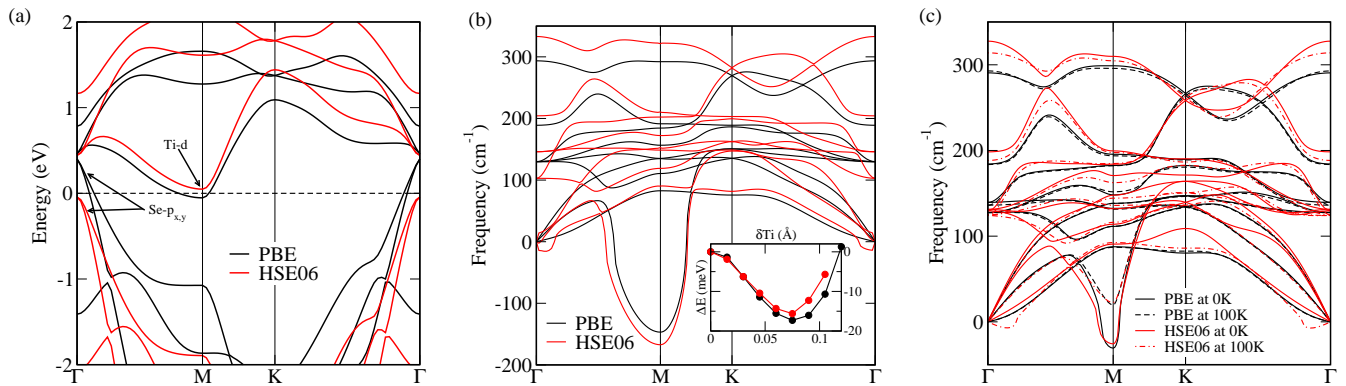


FIG. 2. (a) Electronic bands from PBE and HSE06 approximations. (b) The harmonic phonon bands calculated on a 4×4 supercell and the energy gain as a function of δTi where ΔE is the energy difference per 2×2 cell. (c) The anharmonic phonon dispersion on a 4×4 supercell at 0 and 100 Kelvin from PBE and HSE06 force engines. PBE and HES06 results are obtained from QUANTUM ESPRESSO and CRYSTAL, respectively.

these quantities can indeed be recasted as appropriate stochastic averages over the atomic forces. As the HSE06 calculation is computationally expensive, we perform the calculation on a 4×4 supercell (i.e., 48 atoms). Even if this supercell size is not completely converged and T_{CDW} is underestimated, as it will be shown later, it is clear from Fig. 2 (c) that PBE and HSE06 yield practically the same low energy dispersion around the M point even with full inclusion of anharmonicity. Moreover, the temperature dependence of the soft mode is also very similar, indicative of a practically identical T_{CDW} (i.e., identified as the point where the energy of the soft phonon at M crosses zero) for the two functionals on the 4×4 cell. Other phonon modes, particularly around zone center, suffer of a somewhat stronger renormalization by exchange (analogous to the harmonic case), however, as we are mainly interested in the CDW transition, we can stick to the PBE functional and proceed with calculations on larger supercells (see [22] for additional technical details and the magnitude of the different terms in Eq. (1)).

The anharmonic phonon spectrum obtained by evaluating Eq. (1) on a 8×8 supercell (i.e., 192 atoms) for several temperatures is shown in Fig. 3. As it can be seen, the harmonic phonon frequency of the lowest energy mode at M is $\omega_{A_{1u}} \approx -135 \text{ cm}^{-1}$, while at 300K the anharmonic phonon frequency of the same mode is $\approx -26 \text{ cm}^{-1}$. Thus, already at room temperature, the anharmonic correction is of the same order of the harmonic phonon frequency. Between 400 and 500K, this phonon mode becomes positive, compatible with a CDW transition within this temperature range. Note that this transition temperature differs substantially with respect to the one on a 4×4 supercell which reflects the importance of cell size. To better illustrate this point, in the inset of Fig. 3 we show the convergence of the soft mode phonon frequency as a function of the cell size at 300K. The A_{1u} phonon frequency at M is fully converged on the 8×8 cell [22]. We can then obtain $T_{\text{CDW}} \approx 440\text{K}$ for a

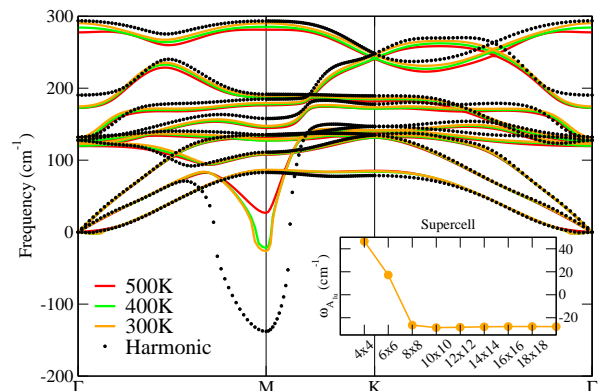


FIG. 3. Harmonic and anharmonic phonon dispersion on a 8×8 supercell. Inset: the convergence of the lowest phonon frequency at the M point $\omega_{A_{1u}}$ with respect to the size of the cell at 300K. The results of the cell larger than 8×8 come from the interpolation method detailed in [22].

suspended and undoped monolayer TiSe_2 .

Our calculated T_{CDW} from first-principles SSCHA is 1.6-2.0 times higher than the measured one (depending on the substrate [14–16, 35]). However, our calculation is for an undoped isolated monolayer, the measured samples are instead supported by the substrate and substantially n -doped. In order to understand the origin of this discrepancy, we investigate the effect of electron-doping to see if it can be responsible for the decrease in T_{CDW} . To this end, we first determine the electron doping amount by performing HSE06 n -doped electronic structure calculations by changing the number of valence electrons and adding a compensating jellium (i.e., the virtual crystal approximation (VCA)) until the bands agree well with the ARPES spectra [19] (see [22] for details). With this electron density (i.e., $4.6 \times 10^{13} \text{ cm}^{-2}$ indicative of a substantial doping), we then perform a PBE linear response harmonic calculation to obtain the harmonic phonon dispersion shown in Fig. 4. It turns out that the harmonic

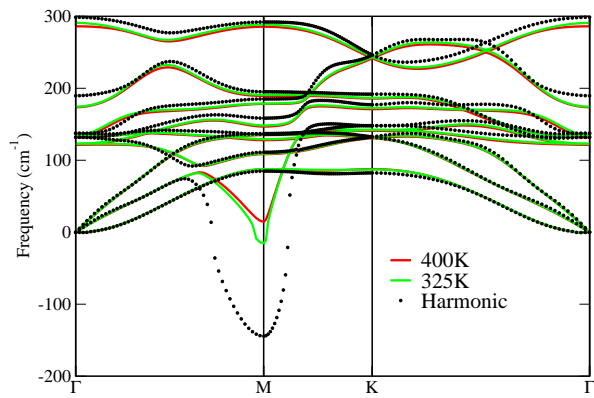


FIG. 4. Harmonic and anharmonic phonon spectra for doped ($n = 4.6 \times 10^{13} \text{cm}^{-2}$) samples calculated on a 8×8 supercell.

phonon dispersion (and consequently the effects of the electron-phonon interaction) are doping independent at this level of doping (by comparing the two black dotted curves in Figs. 3 and 4), consistent with an earlier study [23]. However, when anharmonicity is included, the electron-doping substantially suppresses the CDW instability as illustrated in Fig. 4 leading to $T_{\text{CDW}} \approx 364\text{K}$ for a suspended TiSe_2 monolayer, close to the experimental data of 280K on insulating MoS_2 substrate [14].

In conclusion, we study anharmonic effects in a free-standing TiSe_2 monolayer within the stochastic self-consistent harmonic approximation. We have shown that the electron-hole exchange plays only a marginal role on the vibrational properties of its high- T phase, at odds with its bulk counterpart where the exchange interaction is crucial. We showed that the weakening of the electron-hole interaction in single layer is related to the different periodicity of the modulation with respect to the bulk and the fact that it couples different states in the electronic structure. Our results upturns the conventional wisdom that the electron-hole interaction should be stronger in low dimension due to an increase in binding energy [1–4, 21], mainly because of the strong momentum dependence of the electron-hole interaction and the complex multiband nature of the electronic structure in TiSe_2 . It also underlines that simple qualitative arguments based on the exciton binding energy and its dependence on the effective mass and on the screening (see Eq. (1) in Ref. [1]) do not easily apply since they are unable to explain the occurrence of charge density waves and the temperature dependence of phonon spectra when reducing the dimensionality.

By studying the temperature dependence of the A_{1u} soft mode at the M point, we find the T_{CDW} of an isolated and undoped single-layer to be $\approx 440\text{K}$, while $T_{\text{CDW}} \approx 364\text{K}$ for an electron-doping $n = 4.6 \times 10^{13} \text{cm}^{-2}$, close to the experimental value for supported sample. Thus, T_{CDW} is strongly doping dependent when including anharmonicity, an effect completely absent at the harmonic level as harmonic spectra are weakly doping

dependent. Our work establishes phonon-phonon scattering and the density of carriers in the conduction band as the two mechanisms determining the melting of CDW in a single-layer TiSe_2 .

Computational resources were granted by PRACE (Project No. 2017174186) and from IDRIS, CINES and TGCC (Grant eDARI 91202 and Grand Challenge Jean Zay). We acknowledge support from the Graphene Flagship core 2 (Grant No. 785219) and Agence nationale de la recherche (Grant No. ANR-17-CE24-0030). F. M. and L. M. acknowledge support by the MIUR PRIN-2017 program, project number 2017Z8TS5B. I.E. acknowledges financial support from the Spanish Ministry of Economy and Competitiveness (FIS2016-76617-P). We acknowledge U. Aseguinolaza for useful discussions.

* zhou@insp.jussieu.fr

† matteo.calandra@upmc.fr

- [1] D. Sherrington and W. Kohn, *Rev. Mod. Phys.* **40**, 767 (1968).
- [2] L. V. Keldysh and A. N. Kozlov, *Sov. Phys. JETP* **27**, 521 (1968).
- [3] Y. V. Keldysh, L. V. & Kopaev, *Fiz. Tverd. Tela* **6**, 2791 (1964), [*Sov. Phys. Solid State* **6**, 2219 (1965)].
- [4] D. Jérôme, T. M. Rice, and W. Kohn, *Phys. Rev.* **158**, 462 (1967).
- [5] A. Kogar, M. S. Rak, S. Vig, A. A. Husain, F. Flicker, Y. I. Joe, L. Venema, G. J. MacDougall, T. C. Chiang, E. Fradkin, J. van Wezel, and P. Abbamonte, *Science (New York, N.Y.)* **358**, 1314 (2017).
- [6] M. Calandra and F. Mauri, *Phys. Rev. Lett.* **106**, 196406 (2011).
- [7] F. Weber, S. Rosenkranz, J.-P. Castellan, R. Osborn, G. Karapetrov, R. Hott, R. Heid, K.-P. Bohnen, and A. Alatas, *Phys. Rev. Lett.* **107**, 266401 (2011).
- [8] M. Hellgren, J. Baima, R. Bianco, M. Calandra, F. Mauri, and L. Wirtz, *Phys. Rev. Lett.* **119**, 176401 (2017).
- [9] J. A. Holy, K. C. Woo, M. V. Klein, and F. C. Brown, *Phys. Rev. B* **16**, 3628 (1977).
- [10] C. S. Snow, J. F. Karpus, S. L. Cooper, T. E. Kidd, and T.-C. Chiang, *Phys. Rev. Lett.* **91**, 136402 (2003).
- [11] S. Baroni, S. de Gironcoli, A. Dal Corso, and P. Gianozzi, *Rev. Mod. Phys.* **73**, 515 (2001).
- [12] R. Bianco, M. Calandra, and F. Mauri, *Phys. Rev. B* **92**, 094107 (2015).
- [13] T. Rohwer, S. Hellmann, M. Wiesenmayer, C. Sohr, A. Stange, B. Slomski, A. Carr, Y. Liu, L. M. Avila, M. Kalläne, S. Mathias, L. Kipp, K. Rossnagel, and M. Bauer, *Nature* **471**, 490 (2011).
- [14] S. Kolekar, M. Bonilla, Y. Ma, H. C. Diaz, and M. Batzill, *2D Materials* **5**, 015006 (2018).
- [15] H. Wang, Y. Chen, M. Duchamp, Q. Zeng, X. Wang, S. H. Tsang, H. Li, L. Jing, T. Yu, E. H. T. Teo, and Z. Liu, *Advanced Materials* **30**, 1704382 (2018).
- [16] L. J. Li, E. C. T. O’Farrell, K. P. Loh, G. Eda, B. Özyilmaz, and A. H. Castro Neto, *Nature* **529**, 185 (2016).

- [17] D. L. Duong, G. Ryu, A. Hoyer, C. Lin, M. Burghard, and K. Kern, *ACS Nano* **11**, 1034 (2017).
- [18] K. Sugawara, Y. Nakata, R. Shimizu, P. Han, T. Hitosugi, T. Sato, and T. Takahashi, *ACS Nano* **10**, 1341 (2016), pMID: 26624791, <https://doi.org/10.1021/acs.nano.5b06727>.
- [19] P. Chen, Y. H. Chan, X. Y. Fang, Y. Zhang, M. Y. Chou, S. K. Mo, Z. Hussain, A. V. Fedorov, and T. C. Chiang, *Nature Communications* **6**, 8943 (2015).
- [20] X.-Y. Fang, H. Hong, P. Chen, and T.-C. Chiang, *Phys. Rev. B* **95**, 201409 (2017).
- [21] D. Jérôme, T. M. Rice, and W. Kohn, *Phys. Rev.* **158**, 462 (1967).
- [22] See Supplementary material for theoretical and computational details and for additional results.
- [23] B. Guster, E. Canadell, M. Pruneda, and P. Ordejón, *2D Materials* **5**, 025024 (2018).
- [24] I. Errea, M. Calandra, and F. Mauri, *Phys. Rev. Lett.* **111**, 177002 (2013).
- [25] R. Bianco, I. Errea, L. Paulatto, M. Calandra, and F. Mauri, *Phys. Rev. B* **96**, 014111 (2017).
- [26] I. Errea, M. Calandra, and F. Mauri, *Phys. Rev. B* **89**, 064302 (2014).
- [27] L. Monacelli, I. Errea, M. Calandra, and F. Mauri, *Phys. Rev. B* **98**, 024106 (2018).
- [28] U. Aeginolaza, R. Bianco, L. Monacelli, L. Paulatto, M. Calandra, F. Mauri, A. Bergara, and I. Errea, *Phys. Rev. Lett.* **122**, 075901 (2019).
- [29] R. Bianco, I. Errea, L. Monacelli, M. Calandra, and F. Mauri, *Nano Letters* **19**, 3098 (2019), pMID: 30932501, <https://doi.org/10.1021/acs.nanolett.9b00504>.
- [30] First-principles calculations are carried out using the bulk experimental lattice parameter ($a = 3.5398 \text{ \AA}$) [36]. This value agrees well with the one for single-layer TiSe_2 on top of bilayer graphene [19, 37]. The difference between the theoretical PBE ($a_{\text{PBE}} = 3.5337$) and HSE06 ($a_{\text{HSE06}} = 3.5546$) lattice parameters and experiments is below 0.2% and 0.6%, thus, marginal. We include a 12.01 \AA vacuum region in out-of-plane direction to avoid interaction between periodic images. The atomic positions are fully relaxed using the PBE [38] and HSE06 [39, 40] approximations within DFT as implemented in **QUANTUM ESPRESSO** [41, 42] and **CRYSTAL** [43] packages, respectively. The harmonic phonon bands are computed within DFPT [11] in **QUANTUM ESPRESSO** and finite differences from analytic forces in **CRYSTAL**. Both codes give practically the same electronic and harmonic phonon bands at the PBE level. Anharmonic effects at non-perturbative level are obtained within SSCHA [24–27]. Additional computational details can be found in the supplemental material [22]. Finally, we neglect the spin-orbit coupling (SOC) as its effect on the phonon dispersion is marginal [22].
- [31] P. Chen, Y.-H. Chan, M.-H. Wong, X.-Y. Fang, M. Y. Chou, S.-K. Mo, Z. Hussain, A.-V. Fedorov, and T.-C. Chiang, *Nano Letters* **16**, 6331 (2016), pMID: 27648493, <https://doi.org/10.1021/acs.nanolett.6b02710>.
- [32] B. Singh, C.-H. Hsu, W.-F. Tsai, V. M. Pereira, and H. Lin, *Phys. Rev. B* **95**, 245136 (2017).
- [33] D. Pasquier and O. V. Yazyev, *Phys. Rev. B* **98**, 235106 (2018).
- [34] F. J. Di Salvo, D. E. Moncton, and J. V. Waszczak, *Phys. Rev. B* **14**, 4321 (1976).
- [35] L. Sun, C. Chen, Q. Zhang, C. Sohr, T. Zhao, G. Xu, J. Wang, D. Wang, K. Rossnagel, L. Gu, C. Tao, and L. Jiao, *Angewandte Chemie International Edition* **56**, 8981 (2017).
- [36] C. Riekel, *Journal of Solid State Chemistry* **17**, 389 (1976).
- [37] J.-P. Peng, J.-Q. Guan, H.-M. Zhang, C.-L. Song, L. Wang, K. He, Q.-K. Xue, and X.-C. Ma, *Phys. Rev. B* **91**, 121113 (2015).
- [38] J. P. Perdew, K. Burke, and M. Ernzerhof, *Phys. Rev. Lett.* **77**, 3865 (1996).
- [39] J. Heyd, G. E. Scuseria, and M. Ernzerhof, *The Journal of Chemical Physics* **118**, 8207 (2003), <https://doi.org/10.1063/1.1564060>.
- [40] A. V. Krukau, O. A. Vydrov, A. F. Izmaylov, and G. E. Scuseria, *The Journal of Chemical Physics* **125**, 224106 (2006), <https://doi.org/10.1063/1.2404663>.
- [41] P. Giannozzi, S. Baroni, N. Bonini, M. Calandra, R. Car, C. Cavazzoni, D. Ceresoli, G. L. Chiarotti, M. Cococcioni, I. Dabo, A. D. Corso, S. de Gironcoli, S. Fabris, G. Fratesi, R. Gebauer, U. Gerstmann, C. Gougoussis, A. Kokalj, M. Lazzeri, L. Martin-Samos, N. Marzari, F. Mauri, R. Mazzarello, S. Paolini, A. Pasquarello, L. Paulatto, C. Sbraccia, S. Scandolo, G. Sclauzero, A. P. Seitsonen, A. Smogunov, P. Umari, and R. M. Wentzcovitch, *Journal of Physics: Condensed Matter* **21**, 395502 (2009).
- [42] P. Giannozzi, O. Andreussi, T. Brumme, O. Bunau, M. B. Nardelli, M. Calandra, R. Car, C. Cavazzoni, D. Ceresoli, M. Cococcioni, N. Colonna, I. Carnimeo, A. D. Corso, S. de Gironcoli, P. Delugas, R. A. DiStasio, A. Ferretti, A. Floris, G. Fratesi, G. Fugallo, R. Gebauer, U. Gerstmann, F. Giustino, T. Gorni, J. Jia, M. Kawamura, H.-Y. Ko, A. Kokalj, E. Kçkbenli, M. Lazzeri, M. Marsili, N. Marzari, F. Mauri, N. L. Nguyen, H.-V. Nguyen, A. O. de-la Roza, L. Paulatto, S. Ponc, D. Rocca, R. Sabatini, B. Santra, M. Schlipf, A. P. Seitsonen, A. Smogunov, I. Timrov, T. Thonhauser, P. Umari, N. Vast, X. Wu, and S. Baroni, *Journal of Physics: Condensed Matter* **29**, 465901 (2017).
- [43] R. Dovesi, A. Erba, R. Orlando, C. M. Zicovich-Wilson, B. Civalleri, L. Maschio, M. Rrat, S. Casassa, J. Baima, S. Salustro, and B. Kirtman, *Wiley Interdisciplinary Reviews: Computational Molecular Science* **8**, <https://onlinelibrary.wiley.com/doi/pdf/10.1002/wcms.1360>.